

Synthesis of Copper Peroxide Nanodots for H₂O₂ Self-Supplying Chemodynamic Therapy

Li-Sen Lin,^{†,‡} Tao Huang,^{‡,‡} Jibin Song,^{§,‡} Xiang-Yu Ou,[§] Zhangtong Wang,[†] Hongzhang Deng,[†] Rui Tian,[†] Yijing Liu,[†] Jun-Feng Wang,^{||} Yuan Liu,[†] Guocan Yu,[†] Zijian Zhou,[†] Sheng Wang,^{*,†} Gang Niu,[†] Huang-Hao Yang,^{§,‡} and Xiaoyuan Chen^{*,†,‡}

[†]Laboratory of Molecular Imaging and Nanomedicine (LOMIN), National Institute of Biomedical Imaging and Bioengineering (NIBIB), National Institutes of Health (NIH), Bethesda, Maryland 20892, United States

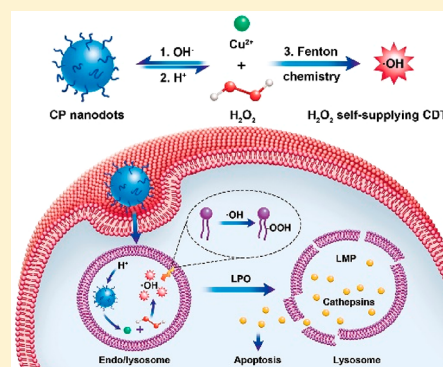
[‡]Department of Radiology, the Fourth Hospital of Harbin Medical University, Harbin, Heilongjiang 150076, P. R. China

[§]MOE Key Laboratory for Analytical Science of Food Safety and Biology, College of Chemistry, Fuzhou University, Fuzhou 350108, P. R. China

^{||}Department of Ultrasound, the First Affiliated Hospital of Harbin Medical University, Harbin, Heilongjiang 150076, P. R. China

Supporting Information

ABSTRACT: Chemodynamic therapy (CDT) employs Fenton catalysts to kill cancer cells by converting intracellular H₂O₂ into hydroxyl radical (•OH), but endogenous H₂O₂ is insufficient to achieve satisfactory anticancer efficacy. Despite tremendous efforts, engineering CDT agents with specific and efficient H₂O₂ self-supplying ability remains a great challenge. Here, we report the fabrication of copper peroxide (CP) nanodot, which is the first example of a Fenton-type metal peroxide nanomaterial, and its use as an activatable agent for enhanced CDT by self-supplying H₂O₂. The CP nanodots were prepared through coordination of H₂O₂ to Cu²⁺ with the aid of hydroxide ion, which could be reversed by acid treatment. After endocytosis into tumor cells, acidic environment of endo/lysosomes accelerated the dissociation of CP nanodots, allowing simultaneous release of Fenton catalytic Cu²⁺ and H₂O₂ accompanied by a Fenton-type reaction between them. The resulting •OH induced lysosomal membrane permeabilization through lipid peroxidation and thus caused cell death via a lysosome-associated pathway. In addition to pH-dependent •OH generation property, CP nanodots with small particle size showed high tumor accumulation after intravenous administration, which enabled effective tumor growth inhibition with minimal side effects in vivo. Our work not only provides the first paradigm for fabricating Fenton-type metal peroxide nanomaterials, but also presents a new strategy to improve CDT efficacy.



INTRODUCTION

Chemodynamic therapy (CDT) is an emerging treatment modality that uses Fenton-type reactions to generate highly cytotoxic hydroxyl radical (•OH), the most active reactive oxygen species (ROS).^{1–6} As known, the formation of •OH via Fenton chemistry relies on the interaction between hydrogen peroxide (H₂O₂) and catalysts, which requires neither oxygen (O₂) nor external energy input. Such a unique pattern of ROS production enables CDT to circumvent the major obstacles of hypoxia-associated resistance and limited light penetration depth in tumor photodynamic therapy,^{7–10} a widely applied ROS-mediated therapeutic strategy.^{11–16} Consequently, much research effort is being devoted to the development of CDT. In recent years, various nanoparticles (NPs) with the capability of controlled Fenton catalyst delivery have been exploited for cancer CDT by employing endogenous H₂O₂ as the substrate of Fenton-type reactions.^{17–21} Nevertheless, although many types of tumor cells have higher intracellular H₂O₂ levels compared with normal cells, the

endogenously produced H₂O₂ is still insufficient to achieve satisfactory chemodynamic efficacy.^{22–24} In this regard, the introduction of H₂O₂-supplementing functionality into CDT agents is highly desirable for enhancing their anticancer efficiency.

There are two different ways to increase intracellular H₂O₂: amplification of endogenous H₂O₂ production in mitochondria, or delivery/generation of exogenous H₂O₂. However, before approaching catalysts to initiate Fenton-type reactions, the endogenous H₂O₂ generated from mitochondria will inevitably undergo rapid decomposition by cellular scavenging enzymes like catalase and peroxidases, resulting in low availability of endogenously increased H₂O₂ for •OH production. Fortunately, exogenous H₂O₂ is possible to be provided near the CDT Fenton catalysts. For example, a polymersome-based nanocarrier was constructed for simulta-

Received: March 30, 2019

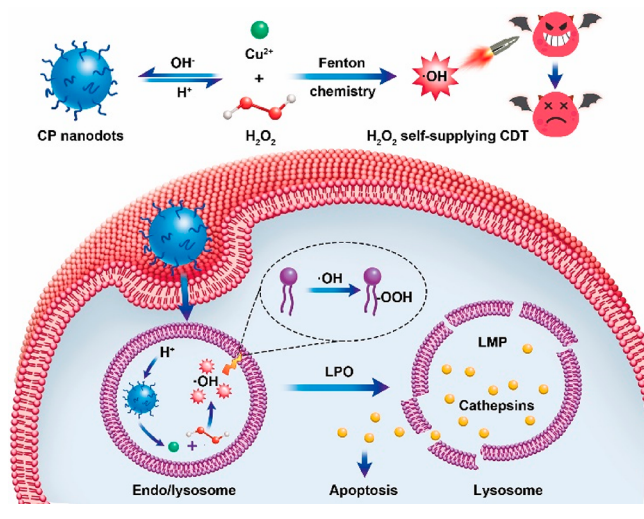
Published: June 2, 2019

neous release of H_2O_2 and Fe_3O_4 nanocatalysts.²⁵ However, external ultrasound was indispensable to trigger the disruption of polymersome. Apart from this, hydrophobic Fe_3O_4 NPs were chosen as the Fenton catalysts to separate them from the liquid H_2O_2 in the hydrophilic core of polymersome, whereas they had poor Fenton catalytic performance compared to hydrophilic ones. Very recently, glucose oxidase (GOx) and its mimics, acting as H_2O_2 producers, have been codelivered with Fe_3O_4 NPs to yield $\bullet\text{OH}$, which meets the requirement of H_2O_2 formation close to Fenton catalysts.^{26,27} Nevertheless, in addition to undesired occurrence during blood circulation, GOx/GOx mimics-mediated conversion of glucose into H_2O_2 and gluconic acid is severely limited by tumor hypoxia due to its O_2 dependence. Thus, there is a great need for more effective CDT agents that are able to specifically and adequately self-provide H_2O_2 around active Fenton-type catalysts without the need of external energy input.

Metal peroxides (MPs) consisting of metal ions and peroxy groups have been proposed as alternative H_2O_2 sources.²⁸ Since several metal ions such as Fe^{2+} , Cu^{2+} , Mn^{2+} , and Co^{2+} have shown excellent Fenton catalytic activity,^{29–32} it is conceivable that Fenton-type metal-based MP NPs may serve as a simple and promising CDT nanoagent able to self-supply H_2O_2 . Recently, although iron peroxide has been obtained under deep lower-mantle conditions (pressure, 76 GPa; temperature, 1800 K), it does not exist when the pressure is decreased below 31 GPa.^{33,34} More importantly, to the best of our knowledge, there is no report on the preparation of Fenton-type metal peroxide nanomaterials.

Herein, we present a facile strategy to synthesize copper peroxide (CP) nanodots as an activatable chemodynamic agent for enhanced CDT by self-supplying H_2O_2 (Scheme 1). With

Scheme 1. Formation of CP Nanodots for H_2O_2 Self-Supplying CDT



the assistance of hydroxide ions (OH^-), CP nanodots were fabricated through the binding of H_2O_2 to Cu^{2+} in the presence of poly(vinylpyrrolidone) (PVP) as stabilizer at room temperature. The role of OH^- is probably to deprotonate H_2O_2 and, thus, to facilitate the coordination of H_2O_2 with Cu^{2+} . The resulting water-insoluble CP could be anchored on the PVP surfactant to obtain PVP-coated CP nanodots with a hydrodynamic diameter of ~ 16.3 nm. The small particle size of CP nanodots allowed them to fully take advantage of the

enhanced permeability and retention (EPR) effect.³⁵ More importantly, the reversible decomposition of CP nanodots into Fenton catalytic Cu^{2+} and H_2O_2 upon acid treatment was followed by a Fenton-like reaction between the decomposition products, endowing them with pH-dependent $\bullet\text{OH}$ production properties. Interestingly, lysosomes, in addition to their unique acidic pH characteristics, are considered to be involved in cell death, because lysosomal membrane permeabilization (LMP) can induce the leakage of lysosomal hydrolases such as cathepsins into the cytosol.^{36–39} After internalization by cancer cells, pH-sensitive CP nanodots were decomposed in the acidic endo/lysosomal compartments, enabling release of abundant H_2O_2 in close proximity to efficient Fenton catalyst and consequent production of downstream highly toxic $\bullet\text{OH}$ which, in turn, caused LMP-mediated cancer cell killing via lysosomal lipid peroxidation (LPO). The anticancer chemodynamic efficacy of CP nanodots was demonstrated both in vitro and in vivo. This study not only provides the first example of a Fenton-type metal peroxide nanoparticle but also highlights the preparation of CP nanodots for H_2O_2 self-supplying CDT.

RESULTS AND DISCUSSION

Preparation and Characterization of CP Nanodots.

The CP nanodots were prepared by the reaction of copper(II) chloride (CuCl_2), H_2O_2 , and sodium hydroxide (NaOH) in an aqueous solution containing PVP at room temperature for 30 min (Figure 1a). The transmission electron microscopy (TEM) images showed that the obtained CP nanodots have a small size of about 5 nm (Figures 1b and S1–S3 of the Supporting Information, SI). The PVP-coated CP nanodots could be well-dispersed in water with a mean hydrodynamic diameter of ~ 16.3 nm (Figure 1c,d). The presence of peroxy groups in CP nanodots was confirmed by a potassium permanganate-based colorimetric method. As shown in Figures 1e and S4, the color of permanganate (MnO_4^-) in acidic solution disappeared upon the addition of CP nanodots, which we attribute to the reduction of MnO_4^- to colorless Mn^{2+} by peroxy groups. In contrast, copper oxide (CuO) NPs did not cause the color change. The molar ratio of peroxy groups to Cu^{2+} in CP nanodots analyzed by MnO_4^- titration was 0.92:1. In the X-ray photoelectron spectroscopy (XPS) spectra of CP nanodots (Figures 1f, S5, and S6), two O 1s peaks at 530.7 and 532.5 eV were assigned to $\text{C}=\text{O}$ and $\text{O}-\text{O}$, respectively, suggesting the existence of PVP and peroxy groups. An obvious N 1s peak was observed (Figure 1h), further demonstrating the presence of PVP coating. It is noteworthy that the PVP layer strongly attenuated the XPS signal from CP component due to the limited information depth of XPS. Importantly, the use of PVP stabilizer enabled the fabrication of CP with small particle size (Figure S7). In addition, the valence state of Cu in CP nanodots was +2 since the Cu 2p XPS spectrum displayed two main peaks at 933.5 and 953.5 eV accompanied by two satellite peaks at 942.1 and 962.1 eV, respectively (Figure 1g).

Formation and Decomposition of CP Nanodots.

To explore the role of OH^- in the formation of CP nanodots, we performed the synthesis process with different amounts of NaOH . As can be seen in Figure 2a,b, no obvious color change was observed upon mixing CuCl_2 with H_2O_2 in the absence of NaOH , indicating that CP nanodots could not be obtained without the addition of OH^- . As the molar ratio of NaOH to CuCl_2 increased, more CP nanodots were formed. However, a

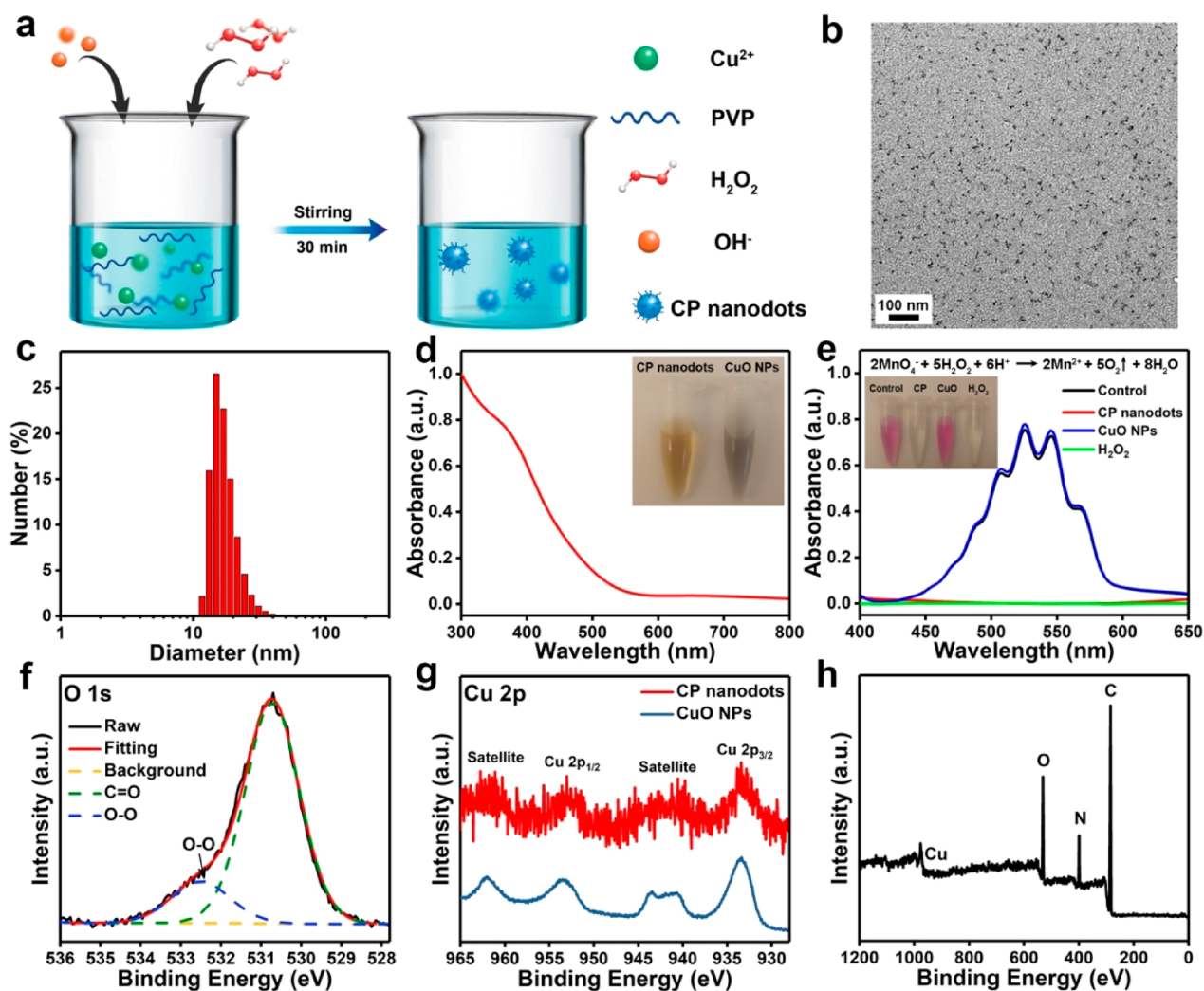


Figure 1. (a) Schematic illustration of the synthetic process of PVP-coated CP nanodots. (b) TEM image, (c) dynamic light scattering (DLS) measurement, and (d) UV-vis absorption spectrum of CP nanodots. (e) Colorimetric analysis demonstrating the presence of peroxy groups in CP nanodots. Peroxy groups can reduce MnO_4^- to colorless Mn^{2+} in strong acidic media (0.1 M H_2SO_4), and thus result in the disappearance of pink color of MnO_4^- . Note that CP nanodots and CuO NPs were quickly dissociated under the acidic condition. (f) High resolution O 1s, (g) Cu 2p, and (h) survey XPS spectra of PVP-coated CP nanodots.

further increase in the ratio to 3:1 resulted in the synthesis of CP nanomaterials with larger size (Figure S8). Furthermore, after the addition of H_2O_2 to CuCl_2 solutions at different pH, CP precipitate was observed at pH 7.4, but not at pH 5.5. Accordingly, the NaOH-assisted formation of CP is likely because the deprotonation of H_2O_2 by OH^- can facilitate its coordination with Cu^{2+} .

Next, we assessed their acid-induced dissociation behavior via measurement of copper (Cu) release. As shown in Figure 2c, a significant Cu release from CP nanodots occurred at pH 5.5, while a relatively slow release was detected at pH 7.4, implying the acid-triggered transformation of CP nanodots into Cu^{2+} and H_2O_2 . The above results demonstrated the pH-responsive decomposition behavior of CP nanodots.

Acid-Induced $\bullet\text{OH}$ Generation from CP Nanodots.

Prior to evaluating the ability of CP nanodots to produce $\bullet\text{OH}$, the generation of $\bullet\text{OH}$ through Fenton-like reaction between Cu^{2+} and H_2O_2 was first determined using the 3,3',5,5'-tetramethylbenzidine (TMB) assay, based on the fact that TMB can be oxidized by the highly reactive $\bullet\text{OH}$ to give a blue-green color with maximum absorbance at about 650 nm.

As can be seen in Figure S9, neither Cu^{2+} nor H_2O_2 alone had a detectable effect on the absorbance increase of TMB even when the incubation duration was extended to 2 h. In contrast, Cu^{2+} plus H_2O_2 led to a rapid color change of TMB aqueous solution (Figures 2d, S10, and S11), thereby confirming excellent Fenton-like catalytic performance of Cu^{2+} and efficient $\bullet\text{OH}$ generation by Cu^{2+} -driven Fenton chemistry.

Considering their acid-induced decomposition, CP nanodots appear to be a smart $\bullet\text{OH}$ generator. As expected, it was found that CP nanodots caused an apparent color change of TMB under mild acidic (pH 5.5) condition, but not under neutral (pH 7.4) condition (Figures 2e and S12). The acid-mediated generation of $\bullet\text{OH}$ by CP nanodots could be ascribed to their dissociation into Cu^{2+} and H_2O_2 at acidic pH as well as the accompanied Fenton-type reaction between these two dissociation products. These results suggested that acidic pH-activatable CP nanodots capable of simultaneously releasing Fenton catalytic Cu^{2+} and H_2O_2 would be promising for cancer treatment through H_2O_2 self-supplying CDT.

In Vitro ROS Generation and CDT Efficacy. Due to the acidic environment of endo/lysosomes, pH-sensitive CP

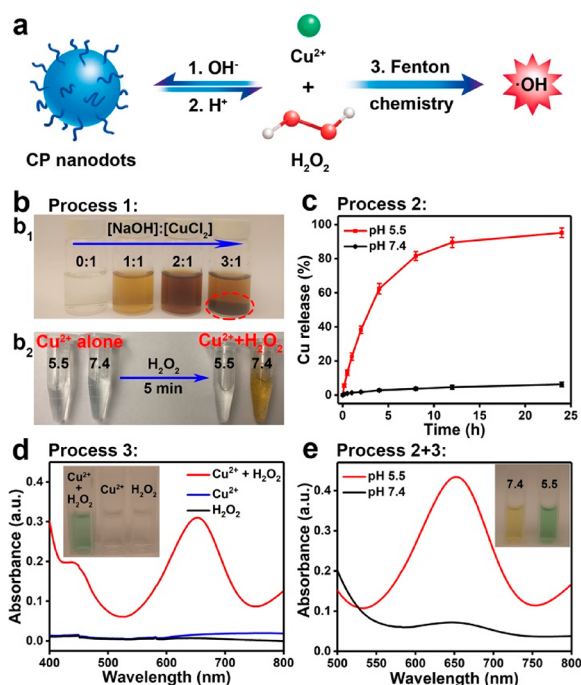


Figure 2. (a) Schematic showing the formation and dissociation of CP nanodots for activatable $\bullet OH$ production. (b₁) Photograph of CP materials obtained in the presence of PVP at different molar ratios of NaOH to CuCl₂. Unexpected precipitation (red circle) was observed during the synthetic process when the ratio was too high (3:1). (b₂) Photograph of CuCl₂ solutions with different pH values before and after the addition of H₂O₂. Note that the CP formed at pH 7.4 was aggregated due to the absence of PVP stabilizer. (c) Cumulative Cu release from CP nanodots in different pH conditions, showing their acid-induced dissociation. (d) UV-vis spectra and photographs (inset) of TMB aqueous solution treated with H₂O₂, Cu²⁺, or Cu²⁺ plus H₂O₂ for 30 min. Note that the weak absorption between 600 and 800 nm at Cu²⁺-treated group is from the CuCl₂. (e) Colorimetric detection of $\bullet OH$ generated by CP nanodots at different pH values based on TMB assay.

nanodots could be decomposed after endocytosis into cancer cells, followed by the Fenton-like reaction between the released Cu²⁺ and H₂O₂. It is worth noting that CP nanodots showed good stability in different physiological media (Figure S13). In order to examine the production of $\bullet OH$ by CP nanodots at the cellular level, 2',7'-dichlorofluorescein diacetate (DCFH-DA) was employed as the fluorescent ROS indicator. Upon crossing the cell membrane, DCFH-DA undergoes deacetylation by intracellular esterases to yield nonfluorescent DCFH, which can be oxidized by ROS and then emits green fluorescence.^{40,41} It can be seen in Figure 3 that U87MG cancer cells incubated with CP nanodots exhibited significantly higher green fluorescence than untreated control cells. Moreover, the ROS-associated fluorescence signal increased with the concentration of CP nanodots (Figure S14). These data indicated the ability of CP nanodots to produce $\bullet OH$ within tumor cells.

Subsequently, the cancer cell killing effect of CP nanodots was investigated by a live/dead cell staining assay. As revealed by fluorescence imaging of calcein AM and propidium iodide (PI) costained U87MG cells (Figure 4a), CP nanodots elicited cancer cell death in a concentration-dependent manner. It has been reported that apoptosis is a major pathway for ROS-mediated cell killing. The apoptotic cells were measured by

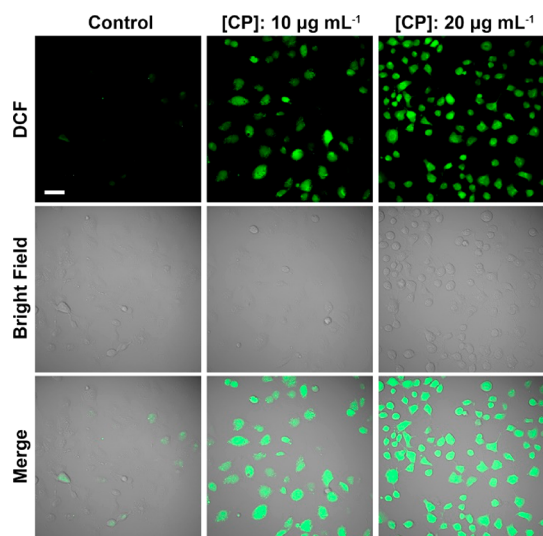


Figure 3. Fluorescence images of DCFH-DA-stained U87MG cancer cells after exposure to different concentrations of CP nanodots for 4 h. The scale bar represents 50 μm .

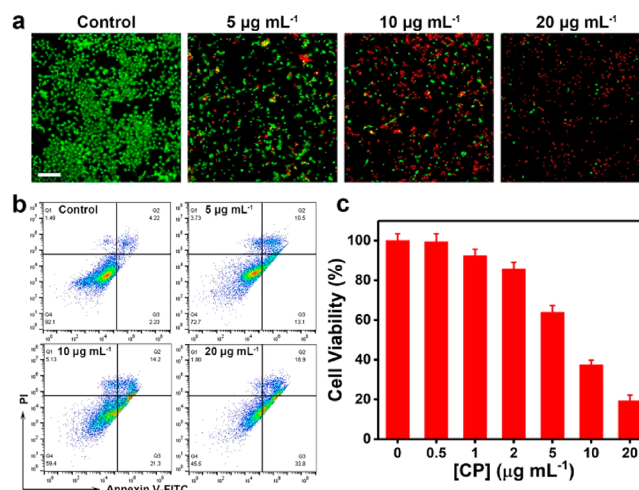


Figure 4. (a) Fluorescence images of calcein AM (green, live cells) and PI (red, dead cells) costained U87MG cells after incubation with various concentrations of CP nanodots for 24 h. The scale bar represents 100 μm . (b) Flow cytometry analysis of apoptosis in U87MG cells treated with CP nanodots for 12 h. (c) In vitro CDT potency of CP nanodots after 24 h of incubation.

flow cytometry using the annexin V-FITC/PI apoptosis detection kit. Obviously, the CP nanodots-treated groups had higher ratios of apoptotic cancer cells compared with control group (Figure 4b). To further quantitatively assess the in vitro chemodynamic efficiency of CP nanodots against U87MG cells, methyl thiazolyl tetrazolium (MTT) assay was performed to test cell viability. As shown in Figure 4c, the cell viability was dramatically decreased to less than 20% when U87MG cells were treated with 20 $\mu g mL^{-1}$ of CP nanodots for 24 h. Additionally, the CP nanodots inhibited tumor cell proliferation in a dose- and time-dependent manner (Figure S15). Intriguingly, CP nanodots exhibited lower toxicity to normal cells (Figure S16). These results confirmed that CP nanodots, serving as an enhanced chemodynamic nanoagent with self-supplied H₂O₂, possess potent anticancer activity.

Therapeutic Mechanism of CP Nanodots-Based CDT. It is well-known that ROS can react with biological molecules

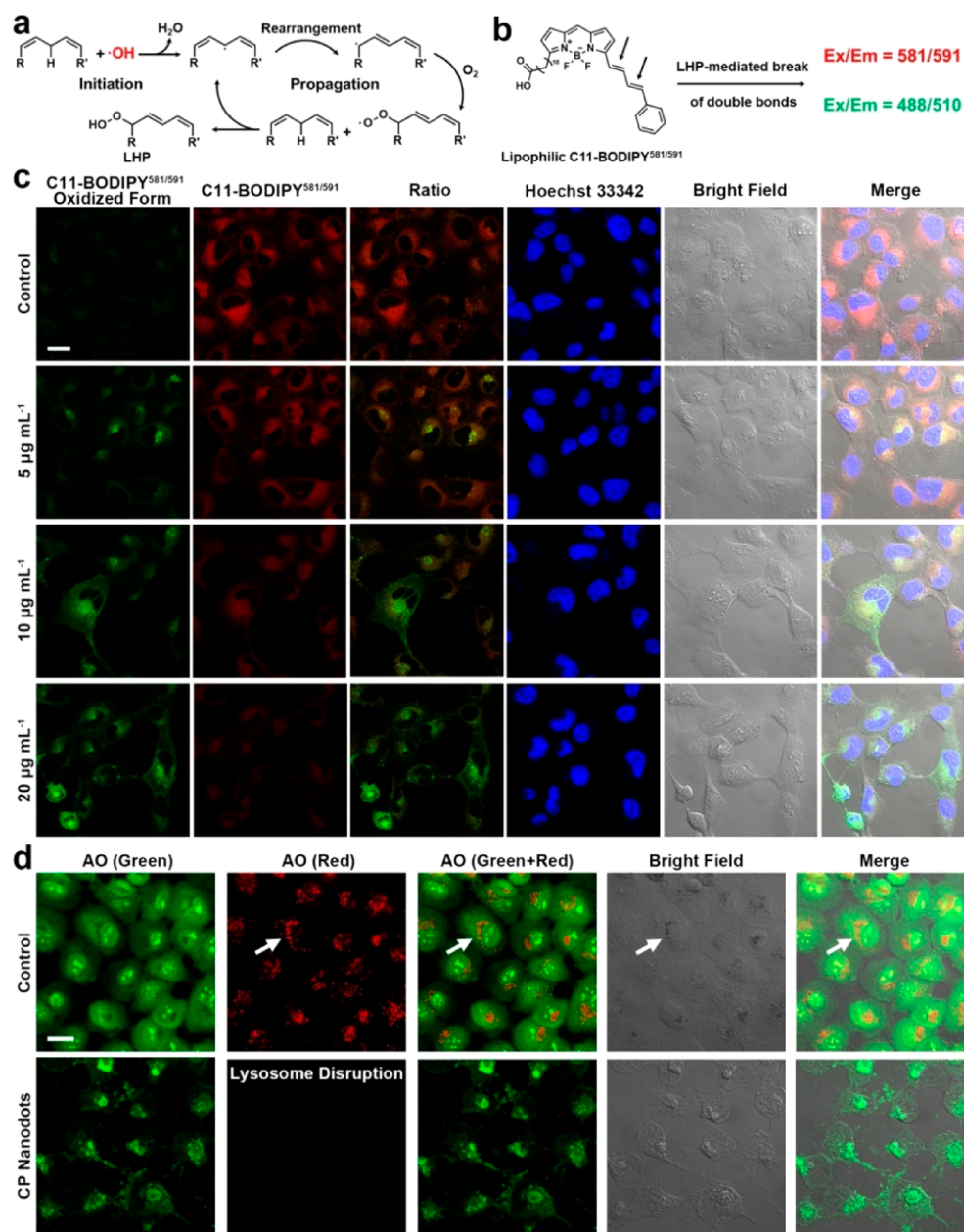


Figure 5. (a) General mechanism for $\bullet\text{OH}$ -initiated LPO, which mainly affects the polyunsaturated lipids containing a 1,4-pentadiene structure because the presence of two double bonds adjacent to a methylene group makes the methylene C–H bond weaker and the resulting bis-allylic radical more stable. (b) Proposed mechanism of the lipophilic C11-BODIPY^{581/591} probe for ratiometric fluorescence imaging of lipid hydroperoxide (LHP), the primary products of LPO. (c) CLSM images of C11-BODIPY^{581/591}-stained U87MG cells treated with various concentrations of CP nanodots for 4 h. The scale bar represents 20 μm . (d) CLSM images of AO-stained U87MG cells incubated with or without CP nanodots for 24 h. The scale bar represents 20 μm . White arrows indicate AO accumulated in intact lysosomes.

including lipids, proteins, and DNA. In particular, $\bullet\text{OH}$ generation by pH-responsive CP nanodots preferentially occurs within the acidic endo/lysosomes, which may give rise to LPO of lysosomal membrane (Figure 5a) and ensuing LMP. To elucidate the CP nanodots-triggered peroxidation of lipids, C11-BODIPY^{581/591} was employed as a ratiometric fluorescent probe. The C11-BODIPY^{581/591} dye is lipophilic and easily penetrates into the lipid bilayer. Its fluorescence shifts from red to green in the existence of lipid hydroperoxide (LHP), the product of lipid peroxidation (Figure 5b). The confocal laser scanning microscopy (CLSM) images revealed that incubation of U87MG cells with CP nanodots before C11-BODIPY^{581/591} staining led to the loss of red fluorescence and

the increase of green fluorescence (Figure 5c), successfully demonstrating the ability of pH-sensitive CP nanodots to cause LPO.

Then, lysosomal membrane integrity of U87MG cells after incubation with CP nanodots was evaluated by the acridine orange (AO) staining method. The AO indicator emits green fluorescence in cytoplasm and nuclei, and emits red fluorescence after accumulation in acidic organelles, particularly intact lysosomes.⁴² As can be seen in Figure 5d, both red and green fluorescence were detected in untreated control cells. In comparison, the red fluorescence was greatly diminished upon the treatment of U87MG cells with CP nanodots, suggesting that lysosomes were damaged, which

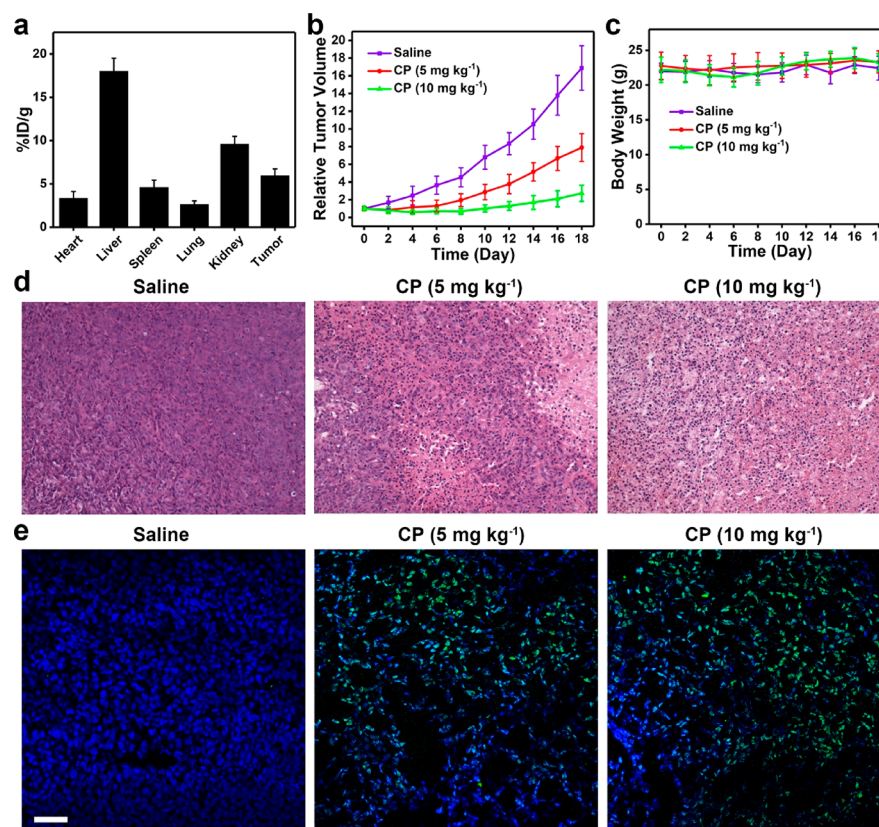


Figure 6. (a) Biodistribution of Cu in major organs and tumor of U87MG tumor-bearing mice at 24 h post i.v. injection with CP nanodots. (b) Relative tumor growth curves of U87MG tumor-bearing mice after treatment with saline (control group) or different doses of CP nanodots. (c) Time-dependent body-weight curves of mice in different groups. (d) H&E-stained images of tumor slices obtained from different groups of mice. (e) Fluorescence images of TUNEL-stained tumor slices after various treatments. Cell nuclei were stained with DAPI (blue fluorescence). Green fluorescence indicates TUNEL-positive cells. The scale bar represents 50 μm .

could be attributed to the acid-triggered $\bullet\text{OH}$ generation by CP nanodots within endo/lysosomes and the ensued lysosomal LPO. Importantly, LMP resulting from the loss of membrane integrity allows the release of lysosomal cathepsins into cytosol and thus elicits cancer cell apoptosis. Accordingly, it can be speculated that one of the most important mechanisms responsible for CP nanodots-mediated cancer cell killing involves lysosomal disruption via $\bullet\text{OH}$ -initiated LPO.

In Vivo CDT Treatment with CP Nanodots. Inspired by the excellent chemodynamic efficacy of CP nanodots in vitro, the in vivo tumor growth inhibition effect was investigated after intravenous (i.v.) administration. It is hypothesized that the PVP-coated CP nanodots with a small hydrodynamic diameter can be effectively accumulated in tumor tissue through the EPR effect. To confirm this, the biodistribution of CP nanodots in U87MG tumor-bearing mice was assessed based on the Cu content measured by inductively coupled plasma optical emission spectrometry (ICP-OES). As expected, the tumor uptake of CP nanodots at 24 h post i.v. injection reached 5.96 ± 0.79 %ID/g (Figure 6a). The high tumor accumulation of CP nanodots makes them suitable for in vivo CDT applications. As can be seen in Figures 6b and S17, mice injected with saline (control group) showed rapid tumor growth, whereas the growth of tumors in CP nanodots-treated mice was significantly suppressed. The remarkable tumor growth inhibition effect of CP nanodots could be ascribed to the effective tumor accumulation as well as their ability of

generating highly toxic $\bullet\text{OH}$ under acidic pH. Moreover, the therapeutic groups of mice receiving i.v. injection of CP nanodots exhibited no apparent change in body weight during the 18 days of observation period (Figures 6c and S18). In addition, there was no noticeable histological damage in the major organs of CP nanodots-treated mice (Figure S19). The therapeutic efficacy was also evidenced by hematoxylin and eosin (H&E) staining which revealed extensive tumor cell death after treatment with CP nanodots (Figure 6d). Subsequently, terminal deoxynucleotidyl transferase-mediated dUTP nick-end labeling (TUNEL) staining was carried out to examine CP nanodots-induced apoptosis in tumor tissue. As shown in Figure 6e, tumors from the therapeutic groups had elevated levels of cell apoptosis compared to that from the saline-treated control group. Therefore, the above results demonstrated the feasibility of using CP nanodots as a smart chemodynamic agent for cancer therapy in vivo.

CONCLUSIONS

In summary, we have described the synthesis of CP nanodots and their application as an activatable CDT agent with self-supplied H_2O_2 . The OH^- -assisted fabrication of CP nanodots through the coordination of H_2O_2 with Cu^{2+} could be reversed at acidic pH. Upon endocytosis by cancer cells, pH-responsive CP nanodots underwent decomposition into Fenton catalytic Cu^{2+} and H_2O_2 within the acidic endo/lysosomal compartments. The accompanied Fenton-type reaction between the decomposition products generated $\bullet\text{OH}$ to disrupt lysosomal

membrane integrity through the initiation of LPO process, thereby triggering LMP-associated cancer cell death. The CP nanodots with small particle size favorable for the EPR effect exhibited high tumor accumulation which, along with the pH-controlled $\bullet\text{OH}$ production, would provide satisfactory chemodynamic efficacy with minimal side effects in vivo. In addition to being the first example of a Fenton-type metal peroxide nanomaterial, CP nanodots can also act as a H_2O_2 self-supplying CDT agent for effective tumor treatment.

EXPERIMENTAL SECTION

Materials. Poly(vinylpyrrolidone) (PVP, M_w 10 000), copper(II) chloride dihydrate ($\text{CuCl}_2 \cdot 2\text{H}_2\text{O}$), sodium hydroxide (NaOH), hydrogen peroxide (H_2O_2 , 30%), 3,3',5,5'-tetramethylbenzidine (TMB), potassium permanganate (KMnO_4), sulfuric acid (H_2SO_4), copper oxide nanoparticles (CuO NPs), sodium acetate, acetic acid, MOPS, 2',7'-dichlorofluorescein diacetate (DCFH-DA), calcein AM, propidium iodide (PI), methyl thiazolyl tetrazolium (MTT), and acridine orange (AO, 2% in H_2O) were obtained from Sigma-Aldrich (St. Louis, MO, U.S.A.). Apoptosis kit with annexin V-FITC and PI, Hoechst 33342 solution (20 mM), and lipid peroxidation kit with C11-BODIPY^{581/591} were purchased from Thermo Fisher Scientific (Waltham, MA, U.S.A.).

Synthesis of PVP-Coated CP Nanodots. PVP (0.5 g) was dissolved in an aqueous solution containing $\text{CuCl}_2 \cdot 2\text{H}_2\text{O}$ (5 mL, 0.01 M). Then, NaOH (5 mL, 0.02 M) and H_2O_2 (100 μL) were added sequentially to the above mixture. After stirring for 30 min, the PVP-coated CP nanodots were collected by ultrafiltration and washed with water several times.

To investigate the formation of CP under different pH conditions, $\text{CuCl}_2 \cdot 2\text{H}_2\text{O}$ (1 mM) was dissolved in buffer solutions (pH 5.5 or 7.4). After the addition of H_2O_2 (10 mM), the mixtures were allowed to react for 5 min.

Colorimetric Assay of Peroxo Groups. KMnO_4 (50 $\mu\text{g mL}^{-1}$) was dissolved in an aqueous solution containing H_2SO_4 (0.1 M). The mixture was treated with CP nanodots, CuO NPs, or H_2O_2 for 10 min. Subsequently, the UV-vis spectra were measured from 400 to 650 nm.

pH-Responsive Decomposition of CP Nanodots. The acid-induced dissociation was assessed by measuring copper (Cu) release. The CP nanodots were dialyzed against buffer solutions with different pH values (7.4 or 5.5). The dialysates were collected at predetermined times and the released Cu was detected by ICP-OES.

$\bullet\text{OH}$ Generation by Cu^{2+} -Driven Fenton-Type Reaction. The acetate buffer solution (pH 5.5) containing TMB (40 $\mu\text{g mL}^{-1}$) were mixed with Cu^{2+} (1 mM) plus H_2O_2 (1 mM). The generation of $\bullet\text{OH}$ was determined by the absorption increase at 650 nm. The TMB solutions treated with Cu^{2+} or H_2O_2 alone were used as control groups.

pH-Dependent $\bullet\text{OH}$ Generation by CP Nanodots. The CP nanodots (0.2 mg mL^{-1}) were added to the TMB solutions with different pH values (7.4 or 5.5). After mixing for 2 h, the absorption spectra were measured.

In Vitro ROS Generation. DCFH-DA was employed as a fluorescent ROS probe to indicate CP nanodots-induced oxidative stress. Briefly, U87MGs cells were exposed to CP nanodots with different concentrations (0, 10, and 20 $\mu\text{g mL}^{-1}$) for 4 h. Then, the cells were stained with DCFH-DA (10 μM) for 30 min, and the fluorescence images were recorded.

In Vitro Chemodynamic Efficacy. First, CP nanodots-triggered cancer cell death was investigated by calcein AM/PI costaining assay. U87MG cells were treated with CP nanodots (0, 5, 10, and 20 $\mu\text{g mL}^{-1}$) for 24 h. After washing twice with PBS, the cells were incubated with calcein AM (1 $\mu\text{g mL}^{-1}$) and PI (1 $\mu\text{g mL}^{-1}$) for 30 min before being observed with a fluorescence microscope.

Cancer cell apoptosis was evaluated by flow cytometric analysis. U87MG cells (2×10^5) were incubated with different concentrations of CP nanodots for 12 h. Afterward the cells were harvested using

trypsin-EDTA and stained with annexin V-FITC/PI for 15 min, followed by flow cytometry to identify the apoptotic cells.

The MTT assay was conducted to quantitatively assess the CDT efficiency. U87MG cells were seeded in 96-well plates at a density of 5000 cells per well. After overnight incubation, the cells were treated with CP nanodots (0–20 $\mu\text{g mL}^{-1}$) for 24 h. Then, the cells were incubated with MTT (1 mg mL^{-1}) for 4 h. After removing the culture medium, DMSO (150 μL) was added and the absorbance at 570 nm was measured.

Lipid Peroxidation Initiated by CP nanodots. U87MG cells plated on confocal dishes were exposed to CP nanodots for 4 h. After washing twice with PBS, the cells were stained with C11-BODIPY^{581/591} dye (10 μM) for 30 min. Hoechst 33342 staining (5 $\mu\text{g mL}^{-1}$, 15 min) was performed to indicate cell nuclei before observation with CLSM.

Lysosomal Membrane Permeabilization. U87MG cells were seeded in confocal dishes and incubated for 24 h. After 24 h of treatment with CP nanodots, the cells were stained with AO (5 μM) for 30 min and then imaged with CLSM. Excitation: 488 nm; Emission: 515–545 nm for green channel, 610–640 nm for red channel.

In Vivo Chemodynamic Therapy. For biodistribution study, CP nanodots were injected into U87MG tumor-bearing mice through the tail vein. At 24 h postinjection, the mice were sacrificed. The tumors and major organs were collected, weighed, and digested in nitric acid. The Cu contents were measured by ICP-OES. Mice injected with saline served as a control.

For in vivo CDT, mice bearing U87MG tumors ($\sim 60 \text{ mm}^3$) were intravenously injected with CP nanodots in saline (5 or 10 mg kg^{-1}) every other day for four doses. The tumor size and body weight were monitored every 2 days. After 18 days of observation, the mice were sacrificed for histological examination.

ASSOCIATED CONTENT

Supporting Information

The Supporting Information is available free of charge on the ACS Publications website at DOI: 10.1021/jacs.9b03457.

Additional experimental results as presented in Figures S1–S19 (PDF)

AUTHOR INFORMATION

Corresponding Authors

*sheng.wang@nih.gov

*shawn.chen@nih.gov

ORCID

Jibin Song: 0000-0003-4771-5006

Huang-Hao Yang: 0000-0001-5894-0909

Xiaoyuan Chen: 0000-0002-9622-0870

Author Contributions

[†]L.-S.L. and T.H. contributed equally to this work.

Notes

The authors declare no competing financial interest.

ACKNOWLEDGMENTS

This work was supported by the National Natural Science Foundation of China (81301255), and the Intramural Research Program (IRP) of the NIBIB, NIH.

REFERENCES

- (1) Ma, B.; Wang, S.; Liu, F.; Zhang, S.; Duan, J.; Li, Z.; Kong, Y.; Sang, Y.; Liu, H.; Bu, W.; Li, L. Self-Assembled Copper-Amino Acid Nanoparticles for in Situ Glutathione "AND" H_2O_2 Sequentially Triggered Chemodynamic Therapy. *J. Am. Chem. Soc.* **2019**, *141*, 849–857.

- (2) Lin, L.-S.; Song, J.; Song, L.; Ke, K.; Liu, Y.; Zhou, Z.; Shen, Z.; Li, J.; Yang, Z.; Tang, W.; Niu, G.; Yang, H.-H.; Chen, X. Simultaneous Fenton-like Ion Delivery and Glutathione Depletion by MnO₂-Based Nanoagent to Enhance Chemodynamic Therapy. *Angew. Chem., Int. Ed.* **2018**, *57*, 4902–4906.
- (3) Tang, Z.; Zhang, H.; Liu, Y.; Ni, D.; Zhang, H.; Zhang, J.; Yao, Z.; He, M.; Shi, J.; Bu, W. Antiferromagnetic Pyrite as the Tumor Microenvironment-Mediated Nanoplatform for Self-Enhanced Tumor Imaging and Therapy. *Adv. Mater.* **2017**, *29*, 1701683.
- (4) Zhang, L.; Wan, S.-S.; Li, C.-X.; Xu, L.; Cheng, H.; Zhang, X.-Z. An Adenosine Triphosphate-Responsive Autocatalytic Fenton Nanoparticle for Tumor Ablation with Self-Supplied H₂O₂ and Acceleration of Fe(III)/Fe(II) Conversion. *Nano Lett.* **2018**, *18*, 7609–7618.
- (5) Fan, J.-X.; Peng, M.-Y.; Wang, H.; Zheng, H.-R.; Liu, Z.-L.; Li, C.-X.; Wang, X.-N.; Liu, X.-H.; Cheng, S.-X.; Zhang, X.-Z. Engineered Bacterial Bioreactor for Tumor Therapy via Fenton-Like Reaction with Localized H₂O₂ Generation. *Adv. Mater.* **2019**, *31*, 1808278.
- (6) Ranji-Burachaloo, H.; Gurr, P. A.; Dunstan, D. E.; Qiao, G. G. Cancer Treatment through Nanoparticle-Facilitated Fenton Reaction. *ACS Nano* **2018**, *12*, 11819–11837.
- (7) Kim, J.; Cho, H. R.; Jeon, H.; Kim, D.; Song, C.; Lee, N.; Choi, S. H.; Hyeon, T. Continuous O₂-Evolving MnFe₂O₄ Nanoparticle-Anchored Mesoporous Silica Nanoparticles for Efficient Photodynamic Therapy in Hypoxic Cancer. *J. Am. Chem. Soc.* **2017**, *139*, 10992–10995.
- (8) Li, X.; Lee, D.; Huang, J.-D.; Yoon, J. Phthalocyanine-Assembled Nanodots as Photosensitizers for Highly Efficient Type I Photo-reactions in Photodynamic Therapy. *Angew. Chem., Int. Ed.* **2018**, *57*, 9885–9890.
- (9) Lan, G.; Ni, K.; Veroneau, S. S.; Feng, X.; Nash, G. T.; Luo, T.; Xu, Z.; Lin, W. Titanium-Based Nanoscale Metal–Organic Framework for Type I Photodynamic Therapy. *J. Am. Chem. Soc.* **2019**, *141*, 4204–4208.
- (10) Chen, H.; Tian, J.; He, W.; Guo, Z. H₂O₂-Activatable and O₂-Evolving Nanoparticles for Highly Efficient and Selective Photodynamic Therapy against Hypoxic Tumor Cells. *J. Am. Chem. Soc.* **2015**, *137*, 1539–1547.
- (11) Huang, L.; Li, Z.; Zhao, Y.; Zhang, Y.; Wu, S.; Zhao, J.; Han, G. Ultralow-Power Near Infrared Lamp Light Operable Targeted Organic Nanoparticle Photodynamic Therapy. *J. Am. Chem. Soc.* **2016**, *138*, 14586–14591.
- (12) Luby, B. M.; Walsh, C. D.; Zheng, G. Advanced Photosensitizer Activation Strategies for Smarter Photodynamic Therapy Beacons. *Angew. Chem., Int. Ed.* **2019**, *58*, 2558–2569.
- (13) Lovell, J. F.; Liu, T. W. B.; Chen, J.; Zheng, G. Activatable Photosensitizers for Imaging and Therapy. *Chem. Rev.* **2010**, *110*, 2839–2857.
- (14) Dong, Z.; Feng, L.; Hao, Y.; Chen, M.; Gao, M.; Chao, Y.; Zhao, H.; Zhu, W.; Liu, J.; Liang, C.; Zhang, Q.; Liu, Z. Synthesis of Hollow Biomaterialized CaCO₃-Polydopamine Nanoparticles for Multimodal Imaging-Guided Cancer Photodynamic Therapy with Reduced Skin Photosensitivity. *J. Am. Chem. Soc.* **2018**, *140*, 2165–2178.
- (15) Lin, L.-S.; Song, J.; Yang, H.-H.; Chen, X. Yolk-Shell Nanostructures: Design, Synthesis, and Biomedical Applications. *Adv. Mater.* **2018**, *30*, 1704639.
- (16) Bai, J.; Jia, X.; Zhen, W.; Cheng, W.; Jiang, X. A Facile Ion-Doping Strategy to Regulate Tumor Microenvironments for Enhanced Multimodal Tumor Theranostics. *J. Am. Chem. Soc.* **2018**, *140*, 106–109.
- (17) Zhang, C.; Bu, W.; Ni, D.; Zhang, S.; Li, Q.; Yao, Z.; Zhang, J.; Yao, H.; Wang, Z.; Shi, J. Synthesis of Iron Nanometallic Glasses and Their Application in Cancer Therapy by a Localized Fenton Reaction. *Angew. Chem., Int. Ed.* **2016**, *55*, 2101–2106.
- (18) Cao, Z.; Zhang, L.; Liang, K.; Cheong, S.; Boyer, C.; Gooding, J. J.; Chen, Y.; Gu, Z. Biodegradable 2D Fe-Al Hydroxide for Nanocatalytic Tumor-Dynamic Therapy with Tumor Specificity. *Adv. Sci.* **2018**, *5*, 1801155.
- (19) Dong, Z.; Feng, L.; Chao, Y.; Hao, Y.; Chen, M.; Gong, F.; Han, X.; Zhang, R.; Cheng, L.; Liu, Z. Amplification of Tumor Oxidative Stresses with Liposomal Fenton Catalyst and Glutathione Inhibitor for Enhanced Cancer Chemotherapy and Radiotherapy. *Nano Lett.* **2019**, *19*, 805–815.
- (20) Liu, Y.; Zhen, W.; Wang, Y.; Liu, J.; Jin, L.; Zhang, T.; Zhang, S.; Zhao, Y.; Song, S.; Li, C.; Zhu, J.; Yang, Y.; Zhang, H. One-Dimensional Fe₂P Acts as a Fenton Agent in Response to NIR II Light and Ultrasound for Deep Tumor Synergetic Theranostics. *Angew. Chem., Int. Ed.* **2019**, *58*, 2407–2412.
- (21) Liu, Y.; Zhen, W.; Jin, L.; Zhang, S.; Sun, G.; Zhang, T.; Xu, X.; Song, S.; Wang, Y.; Liu, J.; Zhang, H. All-in-One Theranostic Nanoagent with Enhanced Reactive Oxygen Species Generation and Modulating Tumor Microenvironment Ability for Effective Tumor Eradication. *ACS Nano* **2018**, *12*, 4886–4893.
- (22) Ma, P.; Xiao, H.; Yu, C.; Liu, J.; Cheng, Z.; Song, H.; Zhang, X.; Li, C.; Wang, J.; Gu, Z.; Lin, J. Enhanced Cisplatin Chemotherapy by Iron Oxide Nanocarrier-Mediated Generation of Highly Toxic Reactive Oxygen Species. *Nano Lett.* **2017**, *17*, 928–937.
- (23) Wang, S.; Wang, Z.; Yu, G.; Zhou, Z.; Jacobson, O.; Liu, Y.; Ma, Y.; Zhang, F.; Chen, Z.-Y.; Chen, X. Tumor-Specific Drug Release and Reactive Oxygen Species Generation for Cancer Chemo/Chemodynamic Combination Therapy. *Adv. Sci.* **2019**, *6*, 1801986.
- (24) Liu, Y.; Ji, X.; Tong, W. W. L.; Askhatova, D.; Yang, T.; Cheng, H.; Wang, Y.; Shi, J. Engineering Multifunctional RNAi Nanomedicine To Concurrently Target Cancer Hallmarks for Combinatorial Therapy. *Angew. Chem., Int. Ed.* **2018**, *57*, 1510–1513.
- (25) Li, W.-P.; Su, C.-H.; Chang, Y.-C.; Lin, Y.-J.; Yeh, C.-S. Ultrasound-Induced Reactive Oxygen Species Mediated Therapy and Imaging Using a Fenton Reaction Activable Polymersome. *ACS Nano* **2016**, *10*, 2017–2027.
- (26) Huo, M.; Wang, L.; Chen, Y.; Shi, J. Tumor-Selective Catalytic Nanomedicine by Nanocatalyst Delivery. *Nat. Commun.* **2017**, *8*, 357.
- (27) Gao, S.; Lin, H.; Zhang, H.; Yao, H.; Chen, Y.; Shi, J. Nanocatalytic Tumor Therapy by Biomimetic Dual Inorganic Nanozyme-Catalyzed Cascade Reaction. *Adv. Sci.* **2019**, *6*, 1801733.
- (28) Huang, C.-C.; Chia, W.-T.; Chung, M.-F.; Lin, K.-J.; Hsiao, C.-W.; Jin, C.; Lim, W.-H.; Chen, C.-C.; Sung, H.-W. An Implantable Depot That Can Generate Oxygen in Situ for Overcoming Hypoxia-Induced Resistance to Anticancer Drugs in Chemotherapy. *J. Am. Chem. Soc.* **2016**, *138*, 5222–5225.
- (29) Poyton, M. F.; Sendekci, A. M.; Cong, X.; Cremer, P. S. Cu²⁺ Binds to Phosphatidylethanolamine and Increases Oxidation in Lipid Membranes. *J. Am. Chem. Soc.* **2016**, *138*, 1584–1590.
- (30) Ember, E.; Rothbart, S.; Puchta, R.; van Eldik, R. Metal Ion-Catalyzed Oxidative Degradation of Orange II by H₂O₂. High Catalytic Activity of Simple Manganese Salts. *New J. Chem.* **2009**, *33*, 34–49.
- (31) Xu, A.; Li, X.; Ye, S.; Yin, G.; Zeng, Q. Catalyzed Oxidative Degradation of Methylene Blue by In Situ Generated Cobalt (II)-Bicarbonate Complexes with Hydrogen Peroxide. *Appl. Catal., B* **2011**, *102*, 37–43.
- (32) Tang, Z.; Liu, Y.; He, M.; Bu, W. Chemodynamic Therapy: Tumor Microenvironment-Mediated Fenton and Fenton-like Reactions. *Angew. Chem., Int. Ed.* **2019**, *58*, 946–956.
- (33) Hu, Q.; Kim, D. Y.; Yang, W.; Yang, L.; Meng, Y.; Zhang, L.; Mao, H.-K. FeO₂ and FeOOH under Deep Lower-Mantle Conditions and Earth's Oxygen-Hydrogen Cycles. *Nature* **2016**, *534*, 241–244.
- (34) Liu, J.; Hu, Q.; Kim, D. Y.; Wu, Z.; Wang, W.; Xiao, Y.; Chow, P.; Meng, Y.; Prakapenka, V. B.; Mao, H.-K.; Mao, W. L. Hydrogen-Bearing Iron Peroxide and the Origin of Ultralow-Velocity Zones. *Nature* **2017**, *551*, 494–497.
- (35) Davis, M. E.; Chen, Z.; Shin, D. M. Nanoparticle Therapeutics: An Emerging Treatment Modality for Cancer. *Nat. Rev. Drug Discovery* **2008**, *7*, 771–782.
- (36) Fehrenbacher, N.; Jaattela, M. Lysosomes as Targets for Cancer Therapy. *Cancer Res.* **2005**, *65*, 2993–2995.
- (37) Boya, P.; Kroemer, G. Lysosomal Membrane Permeabilization in Cell Death. *Oncogene* **2008**, *27*, 6434–6451.

(38) Tian, J.; Ding, L.; Ju, H.; Yang, Y.; Li, X.; Shen, Z.; Zhu, Z.; Yu, J.-S.; Yang, C. J. A Multifunctional Nanomicelle for Real-Time Targeted Imaging and Precise Near-Infrared Cancer Therapy. *Angew. Chem., Int. Ed.* **2014**, *53*, 9544–9549.

(39) Tian, J.; Ding, L.; Xu, H.-J.; Shen, Z.; Ju, H.; Jia, L.; Bao, L.; Yu, J.-S. Cell-Specific and pH-Activatable Rubyrin-Loaded Nanoparticles for Highly Selective Near-Infrared Photodynamic Therapy against Cancer. *J. Am. Chem. Soc.* **2013**, *135*, 18850–18858.

(40) Lin, L.-S.; Cong, Z.-X.; Li, J.; Ke, K.-M.; Guo, S.-S.; Yang, H.-H.; Chen, G.-N. Graphitic-phase C_3N_4 Nanosheets as Efficient Photosensitizers and pH-Responsive Drug Nanocarriers for Cancer Imaging and Therapy. *J. Mater. Chem. B* **2014**, *2*, 1031–1037.

(41) Wang, Z.; Zhang, Y.; Ju, E.; Liu, Z.; Cao, F.; Chen, Z.; Ren, J.; Qu, X. Biomimetic Nanoflowers by Self-Assembly of Nanozymes to Induce Intracellular Oxidative Damage against Hypoxic Tumors. *Nat. Commun.* **2018**, *9*, 3334.

(42) Li, M.; Xia, J.; Tian, R.; Wang, J.; Fan, J.; Du, J.; Long, S.; Song, X.; Foley, J. W.; Peng, X. Near-Infrared Light-Initiated Molecular Superoxide Radical Generator: Rejuvenating Photodynamic Therapy against Hypoxic Tumors. *J. Am. Chem. Soc.* **2018**, *140*, 14851–14859.